IOPscience iopscience.iop.org

Home Search Collections Journals About Contact us My IOPscience

Comparison of fluctuation electron microscopy theories and experimental methods

This article has been downloaded from IOPscience. Please scroll down to see the full text article.

2007 J. Phys.: Condens. Matter 19 455203

(http://iopscience.iop.org/0953-8984/19/45/455203)

View the table of contents for this issue, or go to the journal homepage for more

Download details:
IP Address: 129.252.86.83
The article was downloaded on 29/05/2010 at 06:30

Please note that terms and conditions apply.

IOP PUBLISHING JOURNAL OF PHYSICS: CONDENSED MATTER

J. Phys.: Condens. Matter **19** (2007) 455203 (11pp) doi:10.1088/0953-8984/19/45/455203

Comparison of fluctuation electron microscopy theories and experimental methods

W G Stratton and P M Voyles

Department of Materials Science and Engineering, University of Wisconsin–Madison, Madison, WI, USA

Received 30 July 2007, in final form 31 July 2007
Published 24 October 2007
Online at stacks.iop.org/JPhysCM/19/455203

Abstract
Fluctuation electron microscopy (FEM) experiments to measure nanoscale structural order in amorphous materials come in two types: variable coherence and variable resolution. Either type can be implemented experimentally using either dark-field transmission electron microscope (TEM) imaging or nanodiffraction in a scanning TEM (STEM). We propose that the discrepancy in the magnitude between FEM signals measured with TEM and STEM is caused by a difference in coherence in the two methods. We also compare the nanoscale order length scales extracted from variable-resolution FEM data using the correlation length method proposed by Gibson *et al* and a method we recently proposed based on an explicit cluster model for nanoscale structural order in amorphous materials.

1. Introduction

1.1. Nanoscale structure in amorphous materials

Understanding the atomic structure of amorphous materials is a difficult task. Without the long-range order of a crystal to provide a conceptual framework and baseline idealized structure, it is difficult to define defects, and difficult even to know what structural features are important. Amorphous materials have some order imposed at the scale of a single bond imposed by the fact that they are made up of atoms, but first-neighbor or even second-neighbor ordering seems unlikely to be the end of the story. That has led to a succession of terms like 'medium-range order', 'intermediate-range order', and 'extended-range order', sometimes used interchangeably, sometimes organized into a hierarchy, to describe structure in between the short-range order imposed by atomic bonding and the long-range order which is not present. This no-man's land is at a length scale of the third to the fifth coordination shell, which for inorganic materials is typically 10–20 Å. (It would be significantly larger for molecular or polymeric glasses.)

This definitional difficulty is compounded by the difficulty of measuring the structure of amorphous materials, especially at the nanometer length scale. The most common and

© 2007 IOP Publishing Ltd Printed in the UK

successful structural tool is diffraction. Diffraction measures the sample structure factor, which is uniquely related by a Fourier transform to the pair (or radial) distribution function (PDF) [1, 2]. The PDF is the number of atoms that sit a distance r away from the average atom in the sample. With the advent of high brilliance third-generation synchrotron light sources and intense neutron sources, as well as new methods for structure factor analysis based for example on wavelets [3], diffraction has become an accurate, quantitatively exact tool for characterization of amorphous materials. It also provides the single most important constraint on the other common method of understanding structure in amorphous materials, computer modeling. A computer model of an amorphous material that does not match the measured structure factor is suspect at best.

Despite this, there is good reason to suspect that the structure factor or PDF does not tell the whole story. Formally, there exists an infinite number of structures consistent with any given PDF. One way to quantify their differences is in terms of higher-order atom position correlation functions involving three, four, or more atoms, which can change independently of the two-body function. This suggests a definition of medium-range order (MRO) as non-trivial three- and four-body functions, and we have shown that those functions have higher sensitivity to structure at the 10–20 Å range than the PDF [4, 5]. Even with the three- and four-body function specified, however, the structure is still not formally unique like a crystal, so the question becomes: *What structure is important*? We propose that the important structure is that which has some influence on a material's other measurable properties. There is significant and growing evidence that atomic structure, at a length scale of 10–20 Å, influences electronic properties [6], vibrational modes [7], plastic deformation [8, 9], and crystallization reactions [10].

Since the early days of high-resolution transmission electron microscopy, there has been hope that it might be possible to simply image the structure of amorphous materials with atomic resolution in real space, essentially reading off the atom positions, or at least identifying local structural motifs. It was gradually realized that the early attempts along these lines revealed more about the imperfection of the microscopes than the structure of the sample [11], and van Dyck has recently shown that even with a modern, aberration-corrected, sub-angstrom-resolution electron microscope, the two-dimensional project inherent in this type of experiment makes it impossible to extract atom positions directly [12].

In 1996, Treacy and Gibson realized that the TEM could be useful in another way [13]. (For a thorough recent review, see [14].) Using the TEM's then unique and still unsurpassed ability to mix real space and reciprocal space information, they studied spatial fluctuations in diffracted intensity, in a technique eventually dubbed fluctuation electron microscopy (FEM) [15]. Their first key insight, and what distinguishes FEM from previous TEM-based efforts to study amorphous structure, is that they deliberately configured the microscope for a spatial resolution of 10–20 Å, much larger than the ∼2 Å it was capable of. This matched the resolution of the measurement to the difficult-to-measure, medium-range portion of the sample structure and maximized the spatial fluctuations.

The second key insight was that it was necessary to quantify the magnitude of these fluctuations in order to distinguish meaningful medium-range structure from random, not meaningful structural fluctuations. To this end, they defined the normalized variance,

$$V(k, Q) = \frac{\left\langle I^2(\mathbf{r}, k, Q)\right\rangle - \langle I(\mathbf{r}, k, Q)\rangle^2}{\langle I(\mathbf{r}, k, Q)\rangle^2}, \tag{1}$$

where $I(\mathbf{r}, k, Q)$ is the diffracted intensity as a function of position $\mathbf{r}$ on the sample, scattering vector magnitude k, and the resolution of the experiment $R = 0.61/Q$, with Q being the radius of the objective aperture in reciprocal space. The brackets $\langle\rangle$ indicate averaging over $\mathbf{r}$.

Qualitatively, $V(k, Q)$ is a measure of the structural heterogeneity of the sample at the length scale of the resolution R: if the sample structure is homogeneous, V will be small. If it is heterogeneous, V will be large. If V is large for some k, there must be some almost-planar arrangements of atoms causing diffraction in the direction defined by k, and those pseudo-planes must have spatial extent limited to 10–20 Å. Formally, V, through $\langle I^2 \rangle$, is connected to the three- and four-body atom position distribution functions [15], which have been shown to more strongly encode information at the medium-range length scale of 10–30 Å than the PDF [4, 5].

Experimentally, FEM comes in two flavors [15]. In variable-coherence (VC) FEM, we systematically vary k at constant Q. This probes one medium-range spatial scale, set by Q at typically 15 Å, but many possible pseudo-planar spacings within that medium-range scale. In variable-resolution (VR) FEM, we systematically vary Q at constant k. This selects a single pseudo-planar spacing, and seeks to measure its medium-range spatial extent. Systematically varying k and Q would create a 'fluctuation map'. Either flavor can be realized in one of two TEM modes, as shown in figure 1. In dark-field TEM imaging, $I(k, Q, \mathbf{r})$ is acquired in the form of a real-space image, which has one k, one Q, and many $\mathbf{r}$. k and Q are then changed, and another image is acquired. In STEM nanodiffraction, $I(k, Q, \mathbf{r})$ is acquired in the form of an electron diffraction pattern acquired with a nanometer-sized probe, which has one Q, one $\mathbf{r}$, and many k. That probe is then stepped across the sample to acquire many $\mathbf{r}$.

The two modes are formally identical by the reciprocity theorem as applied to electron imaging [16, 17], but there are important practical differences. Because TEM FEM acquires the $\mathbf{r}$ samples in parallel, there are many more of them than in nanodiffraction. Because STEM FEM acquires the k samples in parallel, there are more of them than in dark-field imaging. It is also significantly easier to perform VR FEM in an STEM. In the common electron optical design for modern STEMs, nanodiffraction uses a 'virtual' objective aperture, which means that there is at least one lens between the physical aperture and the objective lens. Changing the strength of that lens changes the effective size of the aperture, which varies Q. In TEM imaging there is no extra lens between the physical aperture and the objective lens, so changing Q requires changing the size of the aperture mechanically.

Most of the FEM data published so far is of the VC flavor, acquired in dark-field TEM mode [14]. However, STEM FEM data are becoming available [18, 19], with systematic VR FEM data soon to follow. In this paper, we offer an explanation for the nagging inconsistency in TEM FEM and STEM FEM data on the same sample: while the shapes of the $V(k)$ curves (peak positions, relative heights of maxima) are the same between the two techniques, the absolute magnitude of V varies by almost a factor of ten. We also compare two different methods of extracting length-scale information from VR FEM data. The first was proposed by Gibson *et al* based on correlation functions [15], and the second by Stratton and Voyles based on a new model of FEM for an amorphous/nanocrystal composite sample [20].

1.2. An ordering length scale from fluctuation electron microscopy

One of the fundamental questions about any structural feature is: How big is it? FEM requires variable resolution data to answer that question, and there are two ways to extract an ordering length scale from those data. The first, proposed by Gibson *et al* [15], is based on the connection between $V(k)$ and higher-order correlation functions. They started with the assumption that the functional form of g_4 was a Gaussian decay with a decay length Λ,

$$g_4(r_1, r_2, r) = G_4(r_1, r_2)\mathrm{e}^{-r^2/2\Lambda^2}. \qquad (2)$$

$G_4(r_1, r_2)$ is some unknown function which encodes all of the rest of the information about the sample structure. They then substituted that expression into the g_4-dependent term of $V(k)$,

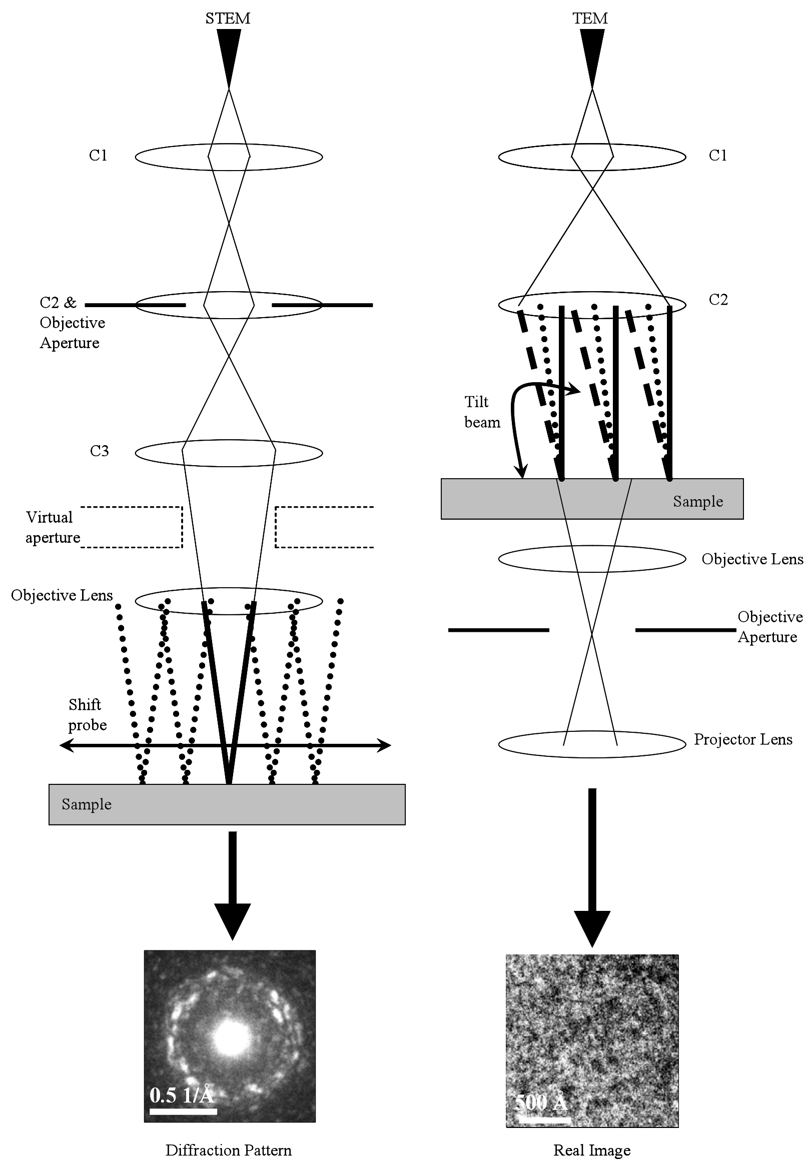

Figure 1. Schematic difference between VR FEM with a STEM and VC FEM with a TEM. VR FEM with a STEM translates the probe to acquire multiple nanodiffraction patterns while VC FEM with a TEM tilts the beam to obtain a real space image. VC FEM with a TEM usually covers multiple more sample area in the V calculation compared to VR FEM.

neglecting the g_3-dependent and g_2-dependent terms as small. The result was an expression for $V(k, Q)$ in which the k-dependent and Q-dependent terms are separable,

$$V(k, Q) = \frac{\Lambda^3 Q^2}{1 + 4\pi^2 Q^2 \Lambda^2} P(k). \tag{3}$$

Λ can then be extracted from the slope and intercept of a line fit to Q^2/V versus Q^2, and all the other details of the structure are subsumed by $P(k)$ [15]. This method worked reasonably

well on simulated FEM data from paracrystalline silicon computer models [15, 21], but has been subjected to only minimal experimental testing [18].

We have taken a different approach to the FEM theory as a whole, and to determining the size of MRO present in a sample in particular [20]. We started by explicitly assuming that the sample structure is an amorphous/nanocrystal composite. This is an idealized form of the paracrystalline MRO found in silicon [22], the crystal-like MRO found in metallic glasses [10] and phase-change chalcogenide thin films [23]. The advantage of making this assumption is that we can parameterize the MRO in the model by the diameter of the nanocrystals, d, and the fraction of the sample volume they occupy, Φ. The result is the expression [20]

$$V = \frac{\left(\frac{\pi}{6}\right) d^3 A_{hkl}\Phi \left(\frac{\pi}{6}d^3\rho - 1\right)^2 \left(1 - \frac{6A_{hkl}\Phi}{\pi}\right)}{R^2 t \left[A_{hkl}\Phi\left(\frac{\pi}{6}d^3\rho - 1\right) + 1\right]^2}, \tag{4}$$

where ρ is the atom number density, R is the resolution of the experiment, and t is the thickness of the sample. A_{hkl} is the fraction of the population of nanocrystals oriented so that their $\{hkl\}$ Bragg reflection is strongly excited. We call this the 'Bragg active fraction', and for randomly oriented, 10–20 Å diameter crystals it is $\sim$0.3, although it varies with the crystal structure, the active reflection, the microscope operating parameters, and the nanocrystal size. This theory uses very simple scattering models for the nanocrystals and the disordered material between them. As a result, the theory does not treat scattering between crystal Bragg conditions, polyatomic systems, or subtle, non-crystal-like MRO. Also, due to the sample structure, the theory is only valid for $R \geqslant d$, which is not true for at least some experiments.

As described in detail elsewhere [20], this theory predicts some simple trends in V with d and Φ. As d increases, so does V. V as a function of Φ, on the other hand, has a maximum in the neighborhood of $A_{hkl}\Phi = 0.1$. We can see qualitatively why this is by considering the extreme values of $A_{hkl}\Phi$. For $A_{hkl}\Phi = 0$, the model is entirely amorphous background, which is the same everywhere, and V must be zero. (In a real sample, the amorphous background will have some small, random structural fluctuations that will lead to residual V, but those are ignored in this simple theory.) For $A_{hkl}\Phi = 1$, the sample is effectively a single crystal. Again, at nanometer spatial resolution, the entire structure is the same, and $V = 0$. In between, the structure is heterogeneous, with a non-zero V, and hence the maximum. We estimate that for most materials studied so far, $A_{hkl}\Phi$ is less than this maximum, except for Al-based metallic glasses [20].

Similarly to the Gibson theory, d can be calculated from the slope of the line fit to V versus R^{-2}. If that slope is Ω, then

$$d = \left(\sqrt{\frac{3}{2\pi}C_{hkl}\Phi t\Omega} + \left(1 + \sqrt{1 + \frac{4}{C_{hkl}\Phi t\Omega\rho}\sqrt{\frac{6t\Omega}{\pi C_{hkl}\Phi}}}\right)\right)^{1/2}, \tag{5}$$

in which $C_{hkl} = A_{hkl}/d$, to make the d-dependence explicit. Equation (5) provides a measure of d provided an independent estimate of Φ is available, or, if $V(R)$ data are available at k corresponding to two different crystal Bragg reflections with significantly different C_{hkl}, d and Φ can both be determined.

2. Experimental details

$Al_{88}Y_7Fe_5$ samples were made via electropolishing using a 25 vol% nitric acid 75 vol% methanol electrolyte in a twin jet electropolisher at 18 V at −40°C. No ion milling was done during the sample preparation, as ion milling has been shown to introduce spurious

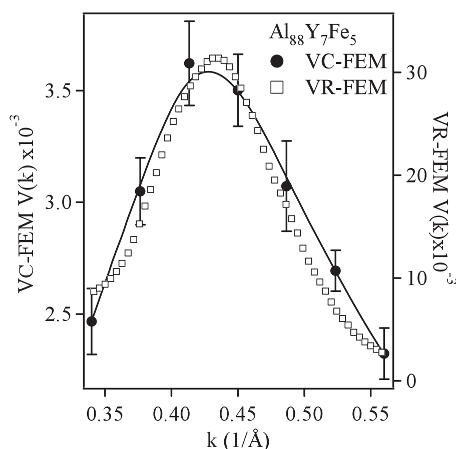

Figure 2. $V(k)$ for $Al_{88}Y_7Fe_5$ by VC and VR FEM. VC FEM (on the TEM) was at 16 Å spatial resolution, and VR FEM (on the STEM) was at 28 Å spatial resolution. While the peak position is conserved between the techniques, VR FEM has values of V that are ten times those of VC FEM.

peaks in V [24]. Thinned samples were viewed within 48 h of electropolishing and kept in a freezer when not in use to minimize possible environmentally caused changes to the amorphous structure.

VC FEM experiments on $Al_{88}Y_7Fe_5$ were done on a LEO 912 energy-filtered TEM at 120 kV and 16 Å spatial resolution. The entire VC FEM curve contains 13 different k values ranging from 0.34 to 0.78.1 Å^{-1}, with each point representing a separate tilt in the TEM. Each k data point is the average of V computed from ten areas on the sample, and reported error bars are the standard deviation of the mean. Each image covers an area of 1500 Å × 1500 Å, which is 8789 16 Å resolution elements (r samples) per image. VR FEM on $Al_{88}Y_7Fe_5$ was done on a FEI Tecnai STEM at 200 kV, with experimental resolutions ranging from 12 to 28 Å. The curve shown in figure 2 is at 28 Å resolution. The VR FEM curve is computed from 100 nanodiffraction patterns with the same probe size from different positions on the sample. Each probe position obtains the entire range of k values at that position r, so there are 512 k points in this measurement. Data on VR FEM experiments on amorphous Si are taken from figure 9 of [18], and VR FEM simulation details are published elsewhere [21].

3. Results and discussion

3.1. TEM FEM versus STEM FEM

In general, $V(k)$ measured using STEM FEM is about an order of magnitude larger than $V(k)$ measured using TEM FEM. An example for $Al_{88}Y_7Fe_5$ is shown in figure 2, and a detailed comparison for a-Ge is given in [18]. If the experiments are formally identical, what causes this difference? We believe that the answer lies in a different degree of coherence in the experimental conditions for the two methods. In STEM, there are two ways to generate nanometer-size probes, which are significantly larger than the ∼2 Å probes routinely achievable in these instruments. One way is to decrease the diameter of the angle-limiting aperture, so that the probe becomes larger due to the diffraction limit. The other way is to decrease the demagnification of the source, which makes the probe larger because the probe is an image of the source. The source-size method results in a probe that has low coherence, while the diffraction-limited probe has high coherence. Various methods to quantify probe coherence

have been proposed [25, 26], and real probes are always some partially coherent mix of source and diffraction-limited size, but STEM FEM, including the data in figure 2 has generally been performed with a high coherence probe, created with large source demagnification and a small field limiting aperture [18].

Coherence in TEM imaging can be adjusted by changing the ratio of the illumination convergence angle β to the objective aperture angle α [17]. Coherence is high for $\beta \ll \alpha$, which is the case for high-resolution TEM imaging. Coherence is low when $\beta \gg \alpha$. The LEO 912 offers an usual degree of control over and reproducibility of the illumination convergence angle, so we are reliably able to perform TEM FEM experiments, such as shown in figure 1, with $\beta = 4$ mrad [10, 20, 27]. The spatial resolution of 16 Å means $\alpha = 0.6$ mrad, placing TEM FEM firmly in the low coherence regime. (A more thorough discussion of coherence in hollow-cone illumination dark-field TEM imaging has been given by Treacy and Gibson [28, 29].) The illumination angle for previous TEM FEM experiments on other microscopes has not been measured, but it is certainly on the order of 1 mrad, $>\alpha$. This large illumination convergence angle is necessary on LaB_6 emitter TEMs to increase the electron intensity on the sample so that exposure times for high-k images do not become too long. (The primary exposure time limitation is sample drift, which must be much smaller than the spatial resolution over the exposure time. This imposes a practical exposure time limit of 30 s on many TEMs.)

The high-coherence STEM probe will be more sensitive to MRO than the low-coherence TEM imaging. Perfectly coherent diffraction from an ordered array of N atoms will result in a diffracted intensity from constructive interference that scales as N^2. Reduced coherence means less enhanced diffracted intensity from MRO, making the ordered region's scattering more like the background scattering, and reducing $V(k)$. Since this difference effects all directions of diffraction equally, the peak locations and relative heights in $V(k)$ are the same in STEM FEM and TEM FEM, but the absolute V is substantially different, as observed in figure 2.

Coherence may also explain the discrepancy in the magnitude of simulated $V(k)$ and experimental $V(k)$. The electron scattering simulations have been performed within the phase-grating [15, 21, 22] and kinematic diffraction [10, 30, 31] approximations, both of which include only coherent scattering, and without including the effects of illumination convergence angle or partial coherence. The result is a simulated $V(k)$ that is significantly too large compared to TEM FEM, but is the right order of magnitude compared to STEM FEM. The match is not quantitative with STEM FEM, but it might be made so with simulated structures with more realistic thickness [32] and structure. It does suggest that FEM simulations compared to high-coherence STEM FEM experiments may avoid the 'Stobbs factor'—the three to ten times over-estimate of contrast in electron micrographs that plagues simulation of high-resolution TEM and high-resolution Z-contrast STEM experiments [33, 34].

3.2. Calculation of MRO sizes using FEM theories

In order to calculate the size of MRO in amorphous materials, we need VR FEM experiments. In the context of our nanocrystal/amorphous composite model, the changing V signal with R (or equivalently, Q) provides a different balance of MRO to amorphous matrix within each resolution element. The only VR FEM data available to us were published by Voyles and Muller [18]. Following Gibson [15], they fit Q^2/V versus Q^2 and found $\Lambda = 11.1$ Å [18]. Since this is a fit of a line to two points, no error was reported.

To apply equation (5) for our new theory, we need to estimate the volume fraction of the nanocrystals (or paracrystals) Φ in the amorphous Si. If we assume that the nanocrystals provide the nucleation sites for crystallization, we can estimate their density from the density of crystals after nucleation but before substantial growth. For silicon grown by sputtering on

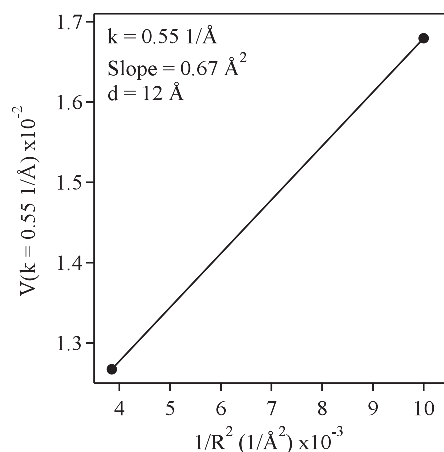

Figure 3. V versus R^{-2} for amorphous Si VR FEM data reported elsewhere [18]. Using the Stratton–Voyles theory, $d = 12$ Å, compared to $\Lambda = 11.1$ Å and a characteristic MRO length of 35 Å calculated in [18] using the Gibson theory.

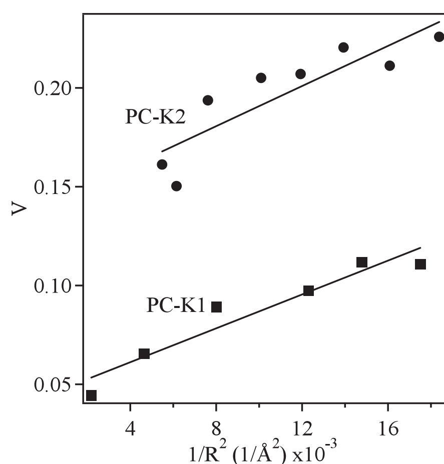

Figure 4. V versus $1/R^2$ for PC-K1 and PC-K2. The solid lines are the fit used to calculate $d = 8.0 \pm 0.2$ and 9.7 ± 0.5 for PC-K1 and PC-K2 respectively using the Stratton–Voyles theory. Resolutions less than 7 Å were neglected.

rock salt, this procedure gives $\Phi = 2.83 \times 10^{-4}$ as a best estimate [20]. Figure 3 shows the plot of V versus R^{-2}, the slope of which, with Φ, gives $d = 12$ Å.

Figure 4 shows the same type of comparison for simulated $V(R)$ data, which are more readily available than experiment. We have used simulations on two paracrystalline silicon models from [21], PC-K1 and PC-K2, the details of which are summarized in table 2 of [21]. Paracrystalline silicon models contain pockets of strained, topologically crystalline Si in an otherwise disordered, continuous random network matrix. PC-K2 has a larger fraction of its atoms in the grains than PC-K1, and thus more order. Treacy *et al* defined as 'topologically crystalline' those atoms for which all the rings of bonds emanating from that atom are in the configuration of a crystal phase [35]. Connected clusters of topologically crystalline atoms define the paracrystalline grains in the model; their diameter is d and their volume fraction in

Table 1. Various measurements of MRO in simulated V from [21] calculated at $k \sim 0.35$ Å. Using Gibson *et al*'s theory, there is the previously published [21] correlation length Λ and the radius of gyration W, along with the calculated nanocrystal diameter d using the Stratton–Voyles theory. The average diameter of the simulated grains is reported as d_{PC}.

Crystal model	Λ (Å)	W (Å)	d (Å)	d_{PC} (Å)
PC-K1	2.5 ± 0.06	7.8 ± 0.2	8.0 ± 0.2	11.4
PC-K2	4.9 ± 0.2	15.4 ± 0.6	9.7 ± 0.5	18.3

the model is Φ. PC-K1 has $d = 11.4$ Å and $\Phi = 0.13$. PC-K2 has $d = 18.3$ Å and $\Phi = 0.57$, so it is more ordered in both ways.

We have replotted Q^2/V versus Q^2 in figure 4 for both PC-K1 and PC-K2. The Gibson theory gives Λ of 2.5 ± 0.06 and 4.9 ± 0.2 Å for PC-K1 and PC-K2 respectively. These numbers are significantly too small to be MRO, so Gibson *et al* suggested treating them as a radius of gyration of a Gaussian-weighted object, which would then have a physical diameter of $W = \sqrt{10}\Lambda$ [15], which is 7.8 ± 0.2 and 15.4 ± 0.6 Å for PC-K1 and PC-K2 respectively. Figure 4 shows V versus R^{-2} for the same models. Given that the Stratton–Voyles theory is only valid for values of the experimental resolution that are greater then d, we only include probe sizes greater than 7 Å. We find $d = 8.0 \pm 0.2$ and 9.7 ± 0.5 Å for PC-K1 and PC-K2 respectively. These results are summarized in table 1.

We now have three measures of the MRO size in these models, all of which show the same trend, but none of which quantitatively agree. Nor is there is a constant scaling factor between any two lengths. This discrepancy returns us to the question of the definition of MRO: the three different measures are sensitive to different aspects of the structure, so while they should probably be correlated, they should not necessarily agree. The topological [21, 35] and correlation length [4, 15, 21] measures have been discussed in detail elsewhere, so we will concentrate on the nanocrystal diameter derived from the new Stratton–Voyles theory. What it really measures is the size of the strongly diffracting regions of the specimen—the spatial extent of the pseudo-planer structures discussed in the introduction. It is consistently smaller than the topological size, which is reasonable. The paracrystallites in these models are strained, so that particularly the outermost atoms in the topologically crystalline clusters are significantly displaced from their ideal crystal lattice positions and contribute less strongly to the diffraction from the cluster. The connection to Λ from the Gibson theory is more difficult to make. Λ reflects both the size and density of ordered regions, and could be sensitive to changes in the matrix between them, or to more subtle, non-cluster types of MRO. This generality is an advantage, but it complicates interpretation.

4. Conclusions

We have compared the two methods of collecting FEM data using dark-field imaging in the TEM and nanodiffraction in the STEM. TEM FEM experiments typically use an imaging mode with little coherence, which we suggest decreases their sensitivity to spatial fluctuations in the sample by decreasing $V(k)$. STEM FEM experiments and FEM simulations have a high degree of coherence, larger $V(k)$, and potentially greater sensitivity. Since the difference between TEM FEM and STEM FEM experiments is instrumental, the relative peak heights and peak positions in V are consistent between the two FEM techniques.

We also compared two methods of extracting the size of MRO regions from variable-resolution (VR) FEM experiments, based on theories of FEM from Gibson *et al* [15] and Stratton and Voyles [20]. The two theories give different but correlated values for the size

of MRO in both FEM simulations and VR FEM experimental data, due to their differing definitions of MRO. Gibson assumes a functional form for g_4, which leads to a very general theory. Stratton and Voyles assume MRO in the form of very small nanocrystals with a well-defined MRO size and volume fraction. The physical interpretation of this theory is more straightforward, but it is less general.

Acknowledgments

We acknowledge J Hamann and J H Perepezko for provision of the $Al_{88}Y_7Fe_5$ samples. This work is supported by NSF under contract DMR-0347746. WGS gratefully acknowledges travel support to the Workshop on Nanoscale Order in Amorphous and Partially Ordered Solids from the International Materials Institute on New Functionality in Glass, DMR-0409588. VR FEM data were acquired in the Electron Microscopy Center at Argonne National Laboratory, which is supported by the Department of Energy Office of Science, with the assistance of Z Y Liu and D J Miller.

References

[1] Cusack N 1987 *The Physics of Structurally Disordered Matter* (Bristol: Institute of Physics Publishing)
[2] Ossi P M 2003 *Disordered Materials; An Introduction* (Heidelberg: Springer)
[3] Uchino T *et al* 2005 Real and reciprocal space structural correlations contributing to the first sharp diffraction peak in silica glass *Phys. Rev.* B **71** 014202
[4] Voyles P M, Gibson J M and Treacy M M J 2000 Fluctuation microscopy: a probe of atomic correlations in disordered materials *J. Electron Microsc.* **49** 259–66
[5] Voyles P M 2001 Fluctuation electron microscopy of medium-range order in amorphous silicon *Physics* (Urbana, Champaign: University of Illinois at Urbana-Champaign)
[6] Nakhmanson S M *et al* 2001 Realistic models of paracrystalline silicon *Phys. Rev.* B **63** 235207
[7] Fortner J and Lannin J S 1988 *Phys. Rev.* B **37** 10154
[8] Falk M L 1999 Molecular-dynamics study of ductile and brittle fracture in model noncrystalline solids *Phys. Rev.* B **60** 7062–70
[9] Hufnagel T C *et al* 2002 Controlling shear band behavior in metallic glass through microstructural design *Intermetallics* **10** 1163–6
[10] Stratton W G *et al* 2005 Aluminum nanoscale order in amorphous $Al_{92}Sm_8$ measured by fluctuation electron microscopy *Appl. Phys. Lett.* **86** (14)
[11] Krivanek O L and Howie A 1975 *J. Appl. Crystallogr.* **8** 213
[12] Dyck D V *et al* 2003 Is atomic resolution transmission electron microscopy able to resolve and refine amorphous structures? *Ultramicroscopy* **98** 27–42
[13] Treacy M M J and Gibson J M 1996 Variable coherence microscopy: a rich source of structural information from disordered systems *Acta Crystallogr.* A **52** 212–20
[14] Treacy M M J *et al* 2005 Fluctuation microscopy: a probe into medium range order *Rep. Prog. Phys.* **68** 2899–944
[15] Gibson J M, Treacy M M J and Voyles P M 2000 Atom pair persistence in disordered materials from fluctuation microscopy *Ultramicroscopy* **83** 169–78
[16] Reimer L 1997 *Transmission Electron Microscopy; Physics of Image Formation and Microanalysis* (*Optical Sciences* vol 36) 4th edn, ed H Lotsch (Berlin: Springer)
[17] Kirkland E J 1998 *Advanced Computing in Electron Microscopy* (New York: Plenum)
[18] Voyles P M and Muller D A 2002 Fluctuation microscopy in the STEM *Ultramicroscopy* **93** 147–59
[19] Nittala L N *et al* 2005 Hydrogen-induced modification of the medium-range structural order in amorphous silicon films *Appl. Phys. Lett.* **87** (24)
[20] Stratton W G and Voyles P M 2007 A phenomenological theory of fluctuation electron microscopy for a nanocrystal/amorphous composite *Ultramicroscopy* submitted
[21] Voyles P M *et al* 2001 Structure and physical properties of paracrystalline atomistic models of amorphous silicon *J. Appl. Phys.* **90** 4437–51
[22] Treacy M M J, Gibson J M and Keblinski P J 1998 Paracrystallites found in evaporated amorphous tetrahedral semiconductors *J. Non-Cryst. Solids* **231** 99–110

[23] Kwon M H *et al* 2007 Nanometer-scale order in amorphous $Ge_2Sb_2Te_5$ analyzed by fluctuation electron microscopy. *Appl. Phys. Lett.* **90** 021923

[24] Li J, Gu X and Hufnagel T C 2003 Using fluctuation microscopy to characterize structural order in metallic glass *Microsc. Microanal.* **9** 509

[25] James E M and Rodenburg J M 1997 Method for measuring the effective source coherence in a field emission transmission electron microscope *Appl. Surf. Sci.* **111** 174–9

[26] Dwyer C *et al* 2007 Electron nanodiffraction using sharply focused parallel probes *Appl. Phys. Lett.* **90** 151104

[27] Stratton W G *et al* 2006 Electron beam induced crystallization of amorphous Al-based alloys in the TEM *Intermetallics* **14** 1061

[28] Treacy M M J and Gibson J M 1993 Coherence and multiple scattering in 'Z-contrast' images *Ultramicroscopy* **52** 31–53

[29] Treacy M M J and Gibson J M 1994 Erratum to 'coherence and multiple scattering in 'Z-contrast' images' *Ultramicroscopy* **54** 93 (erratum)

[30] Khare S V *et al* 2004 Evidence from atomistic simulations of fluctuation electron microscopy for preferred local orientations in amorphous silicon *Appl. Phys. Lett.* **85** 745–7

[31] Dash R K *et al* 2003 A quantitative measure of medium-range order in amorphous materials from transmission electron micrographs *J. Phys.: Condens. Matter* **15** (30)

[32] Bogle S N *et al* 2007 Quantifying nanoscale order in amorphous materials: simulating fluctuation electron microscopy *J. Phys.: Condens. Matter* at press

[33] Boothroyd C B 2000 Quantification of high-resolution electron microscope images of amorphous carbon *Ultramicroscopy* **83** 159–68

[34] Howie A 2004 Hunting the Stobbs factor *Ultramicroscopy* **98** 73–9

[35] Treacy M M J, Voyles P M and Gibson J M 2000 Schläfli cluster topological analysis of medium range order in paracrystalline amorphous semiconductor models *J. Non-Cryst. Solids* **266** 150–5